# A micro-scale model for predicting contact resistance between bipolar plate and gas diffusion layer in PEM fuel cells

Y. Zhou, G. Lin, A.J. Shih, S.J. Hu *

*Department of Mechanical Engineering, The University of Michigan, Ann Arbor, MI 48109-2125, United States*

## Abstract

Contact resistance between the bipolar plate (BPP) and the gas diffusion layer (GDL) in a proton exchange membrane (PEM) fuel cell constitutes a significant portion of the overall fuel cell electrical resistance under the normal operation conditions. Most current methods for contact resistance estimation are experimental and there is a lack of well developed theoretical methods. A micro-scale numerical model is developed to predict the electrical contact resistance between BPP and GDL by simulating the BPP surface topology and GDL structure and numerically determining the status for each contact spot. The total resistance and pressure are obtained by considering all contact spots as resistances in parallel and summing the results together. This model shows good agreements with experimental results. Influences of BPP surface roughness parameters on contact resistance are also studied. This model is beneficial in understanding the contact behavior between BPP and GDL and can be integrated with other fuel cell simulations to predict the overall performance of PEM fuel cells.
© 2006 Published by Elsevier B.V.

*Keywords:* PEM fuel cells; Contact resistance; Surface roughness

## 1. Introduction

Fuel cells are a promising power technology with a wide variety of potential applications. Particularly, proton exchange membrane (PEM) fuel cells have received broad attentions due to their low operation temperature, low emission and quick startup. One of the key technical barriers to the commercialization of PEM fuel cells is the cost-effective manufacturing and precision assembly of fuel cell stacks to achieve the desired performance. One of such performance measures is the cell potential, which decreases from its equilibrium potential during operation because of irreversible losses caused by activation, concentration and ohmic resistances. Among all these resistances, ohmic resistance is dominant under the normal fuel cell operation conditions. Contact resistance constitutes a significant part of the ohmic resistance, especially when stainless steel, titanium or molded graphite is chosen as the BPP material [1,2].

Contact resistance occurs at all interfaces inside the fuel cell, the most important one being at the interface between BPP and GDL, as shown in Fig. 1. Contact resistance is determined by the material properties, surface topology, assembly pressure and operation conditions. During assembly, an optimal assembly pressure is needed to balance the contact resistance and flow resistance in GDL [3]. A high assembly pressure can reduce the contact resistance, but the GDL will be over compressed with high stress, which results in increased flow resistance. Thus, understanding the contact resistance mechanisms between BPP and GDL is important in optimizing clamping pressure as well as improving the fuel cell performance.

Some experimental researches have been conducted on the contact resistance in PEM fuel cell. Mathias et al. [4] showed that contact resistance between GDL and BPP is greater than the bulk resistance of GDL or BPP. Ihonen et al. [5] developed a novel PEM fuel cell assembly to measure the clamping pressure and contact resistances simultaneously for laboratory investigations. Results showed that contact resistances depended on clamping pressure, gas pressure, current density and temperature. Also, the contact resistances of stainless steel could be drastically reduced by surface treatments. Lee et al. [6] measured the PEM fuel cell performance with a variety of commercially available GDLs under various assembly pressures. Each GDL exhibited its own optimal assembly pressure due to the differences in mechanical
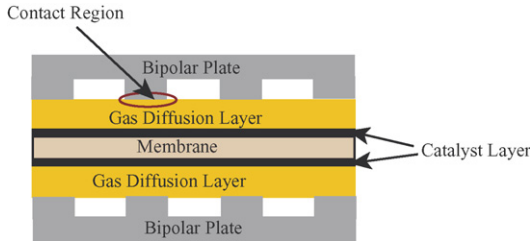
---

Fig. 1. Schematic structure of a PEM fuel cell.

properties and porous characteristics, resulting in different contact resistances in PEM fuel cells.

All of the above-mentioned studies focused on obtaining the contact resistance experimentally. Only a few attempts were made on the development of theoretical models of the contact resistance in PEM fuel cells. Mishra et al. [7] used a fractal based model to predict the contact resistance between GDL and BPP and measured the contact resistance experimentally. However, the GDL surface roughness parameters, which are important inputs for the fractal model, change during compression and are difficult to characterize. In a recent work, Zhang et al. [8] developed simple computational methods for estimating contact resistance between BBP and GDL based on experimentally obtained constitutive resistance–pressure relations.

Despite the lack of theoretical models of contact resistance in PEM fuel cells, a significant amount of literature exists in modeling of electrical contact resistance between contacting bodies. Most of these models incorporate the contact behavior of a single spherical asperity into a statistical model of multi-asperity contact [9–12]. The most recognized one is the Greenwood and Williamson (G&W) statistical model [9], which is based on the Hertz solution for individual elastic contacts and assumes that only asperities originally higher than the separation of the surfaces are in contact. This statistical method accounts for the stochastic nature of the interfacial phenomena and has been widely used to predict the contact of rough surfaces.

This paper develops a micro-scale numerical model to predict the contact resistance between BPP and GDL in PEM fuel cells taking the material properties, surface roughness and clamping pressure as inputs. The classical G&W contact model of rough surfaces is adapted. Experimental measurements of contact resistance between BPP and GDL are also conducted to validate the model. The remainder of the paper is organized as follows: Section 2 introduces the micro-scale contact resistance model, Section 3 describes the numerical example and experiments, Section 4 presents the results and discussions and Section 5 draws the conclusions.

## 2. Micro-scale contact resistance model

In PEM fuel cells, the BPP surface is rough in nature while GDL is a porous medium consisting of randomly distributed fibers. Real contact occurs microscopically between BPP asperities and GDL fibers. Therefore, the topologies of both BPP and GDL are important in understanding their interfacial contact behaviors. The micro-scale contact model is developed using

the following procedure:

(i) The BPP surface topology is simulated as randomly distributed asperities based on measured surface roughness using profilometrical measurements.
(ii) The GDL is modeled as randomly distributed cylindrical fibers with its total fiber length estimated from the GDL porosity and measured fiber diameter.
(iii) Given a nominal separation between the BPP and GDL, BPP asperities in contact with GDL are determined numerically.
(iv) The contact area, force and contact resistance of every single contact spot between BPP and GDL are calculated using the Hertz theory.
(v) The total contact resistance is calculated by considering all contact spots as resistances in parallel and the total clamping force is the summation of the forces on all contact spots.
(vi) Experimental measurements of contact resistance were conducted to validate the modeling results.

### 2.1. BPP surface topology simulation

All surfaces are inherently rough. The surface of a BPP, whether molded using graphite or formed with stainless steel, contains surface roughness, which determines the contact behavior. Consistent with the classical statistical contact models of rough surfaces, the BPP surface is assumed to be covered with asperities whose summits are all spherical in shape with the same radius $R_1$. The summit height follows a normal distribution. The summits are also assumed to be uniformly distributed spatially with a known density $D_{sum}$, measured in "number of summits per unit area". Three parameters, summit radius $R_1$, standard deviation of summit height $\sigma_s$ and summit density $D_{sum}$ are needed to describe the surface roughness. According to McCool [12], a non-dimensional parameter $\alpha$ is introduced,

$$\alpha = \frac{\sigma^2 \sigma''^2_x}{\sigma'^4_x} \tag{1}$$

where $\sigma$, $\sigma'_x$ and $\sigma''_x$ are the root mean square of surface height, slope and second derivative of a surface profile, respectively.

The mean summit radius is expressed as

$$R_1 = \frac{3\pi^{1/2}}{8\sigma''_x} \tag{2}$$

and the variance of the summit height distribution can be calculated from $\sigma$ [11],

$$\sigma_s^2 = \left(1 - \frac{0.8968}{\alpha}\right)\sigma^2 \tag{3}$$

In a two-dimensional surface profile, the local highest point is a peak. The peak density is

$$D_{peak} = \frac{1}{2\pi}\frac{\sigma''_x}{\sigma'_x} \tag{4}$$

The surface profile was obtained using a profilometer with a lateral resolution of 0.5 μm. Several scans in different parts
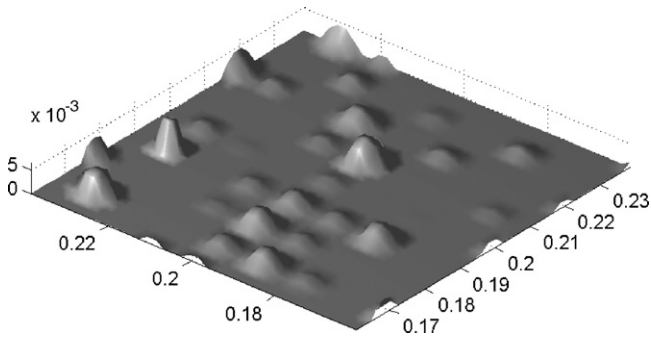
Fig. 2. The generated BPP surface (unit: mm).

of the BPP surface were conduced to obtain one set of roughness parameters for the entire surface. The surface roughness parameters obtained from the average values of several scans are $D_{peak} = 98\ mm^{-1}$, $R_1 = 3.67\ \mu m$ and $\sigma_s = 3.55\ \mu m$.

A three-dimensional surface profile has identical statistical characteristics in every two-dimensional direction. Therefore, the surface summit density is assumed to be $D_{peak}^2$, although it was shown to be slightly larger than $D_{peak}^2$ [12].

According to these surface roughness parameters, a surface profile is generated to simulate the BPP rough surface. A surface is generated with $98 \times 98/mm^2$ randomly distributed spherical summits with $3.67\ \mu m$ in radius. The summit height is normally distributed with a standard deviation of $3.55\ \mu m$. A sample area of the generated surface is illustrated in Fig. 2, which is obtained from one simulation.

This generated surface provides the same surface roughness characteristics as the measured roughness of the real BPP. It also gives the position and height of each asperity summit, which are important inputs for the numerical contact resistance model.

### 2.2. GDL structure simulation

The GDL is made of carbon fiber paper or carbon fiber cloth. The carbon fiber paper is one of the primary materials due to its high porosity (>70%) and good electrical conductivity. It is made from polyacrylonitrile-precursed-carbon fiber, the same material as used for reinforced composite. During the manufacturing process, the chopped carbon fibers are dispersed in water with binders and dried layer by layer to achieve the required thickness. Carbon fibers with a diameter of approximately $7\ \mu m$

and different lengths are randomly distributed to form the carbon fiber paper [4], which can be seen in Fig. 3.

As shown in the SEM micrographs, the GDL used in this study can be approximately treated as a layered structure with binders between fibers. The binder thickness between layers varies at different locations of GDL, from close zero to as much as $6\ \mu m$. The majority of the binder thickness is about $4\ \mu m$. According to the images and assumptions, the carbon fiber paper can be characterized as follows:

- the carbon paper is made of multi-layers of carbon fibers;
- the carbon fiber is cylindrical in shape with a diameter $d_{fiber}$ of approximately $7\ \mu m$;
- the carbon fibers are randomly distributed in length and orientation at each layer;
- the binder thickness $\delta_{binder}$ between two adjacent layers is approximately $4\ \mu m$.

The total fiber length in a unit area of this sample can be obtained as

$$L_{fiber}^{tot} = \frac{V_{GDL} \times (1 - \varepsilon)}{1/4\pi d_{fiber}^2} \tag{5}$$

where $L_{fiber}^{tot}$ is the total fiber length in the unit area, $V_{GDL}$ the volume of the GDL sample and $\varepsilon$ is the porosity. The fiber length in each layer is the total fiber length divided by the number of layers.

$$l_{fiber} = \frac{L_{fiber}^{tot}}{\delta_{GDL}/(d_{fiber} + \delta_{binder})} \tag{6}$$

Based on these characteristics of the carbon fiber paper, one layer of GDL is simulated with randomly distributed carbon fibers, as shown in Fig. 4. The GDL structure is generated as follows: the location of center point and orientation of each fiber varies independently and uniformly in this area. The length of each fiber is assumed to be uniformly distributed from 0 to the diagonal length of this area. When a fiber intersects with existing fibers and boundaries, it is cut at the point of intersection, and the remainder of the fiber turns out to be the new fiber length. Hence, fibers, which appear late have more chance to be cut and become shorter.

The fiber locations and lengths are deterministic for each simulation. Every individual contact spot can be located based
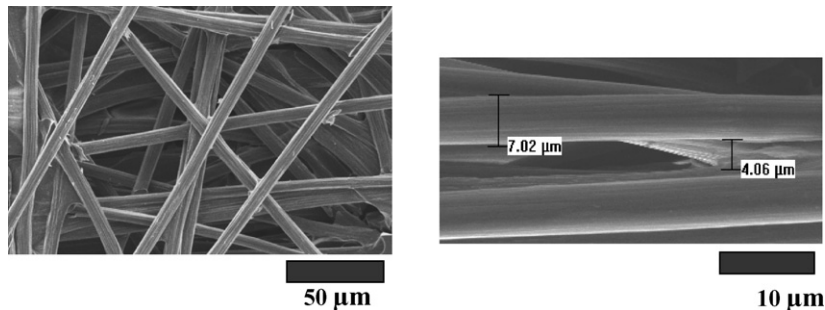


Fig. 3. SEM micrographs of carbon fiber paper.

Fig. 4. Simulation of one layer of carbon fiber in a GDL.

on the information of the relative positions between fibers and BPP asperities.

### 2.3. Contact resistance numerical model

The contact resistance between BPP and GDL is governed by the surface topography and material properties of the contacting pairs. The BPP surface is a rough surface with spherical asperities, which are in the same order of magnitude as the carbon fiber diameter ($\sim 7\,\mu m$). For asperities with heights between 0 and $2\sigma_s$, the contact with GDL is in the first carbon fiber layer. The contact problem is then simplified as asperities contacting with one layer of carbon fibers while neglecting carbon fiber surface roughness.

The behavior of an individual point of contact is known from Hertzian equations [13]. When a cylinder contacts a sphere with nearly the same radius, as in this study, the contact spot is close to a circle and the relation between contact area $a$ and the load $F$ can be expressed approximately in terms of deformation $\delta$ as,

$$a \approx \pi R_e \delta \tag{7}$$

$$F \approx \frac{4}{3} E^* R_e^{1/2} \delta^{3/2} \tag{8}$$

and

$$E^* = \left( \frac{1 - v_1^2}{E_1} + \frac{1 - v_2^2}{E_2} \right)^{-1} \tag{9}$$

where $E_1$, $E_2$, $v_1$, $v_2$ are the Young's moduli and Possion's ratios of the two contacting bodies, respectively. $R_e$ is the equivalent radius of the principal radii of curvature of the surfaces at the contact origin.

$$R_e = R_1 \sqrt{\frac{R_2}{R_1 + R_2}} \tag{10}$$

where $R_2$ denotes the carbon fiber radius.

According to Holm [14], the electrical constriction resistance of this single contact was:

$$R = \frac{\rho_1 + \rho_2}{4r} \tag{11}$$

where $r$ is the radius of the contact area. $\rho_1$ and $\rho_2$ are the resistivities of the two contacting bodies, respectively.

Three basic assumptions for the contact model are made: (1) asperities are far apart and there is no interaction among these asperities; (2) there is no bulk deformation in the bipolar plate; (3) contact is entirely elastic.

Fig. 5 shows a two-dimensional illustration of the relative distance between asperities and fibers. In reality, the fibers are not necessarily parallel and can be located in any direction. O and $O'$ denote the center of spherical asperity and carbon fiber. If the distance $OO'$ is less than the summation of two radii $R_1 + R_2$, the cylinder and the asperity are in contact. Otherwise, there is no contact between them. For a given separation $d$, the deformation between the asperities and fibers is easy to calculate, so the contact area, force and resistance for each contact spot can be determined. The total contact area is the summation of all contact spots and the total contact resistance is calculated by considering the resistance of all contact spots in parallel. The total force is the summation of all contact forces.

## 3. Numerical example and experiments

### 3.1. Numerical example

The above procedure is implemented numerically. A rough BPP surface of $4\,mm \times 4\,mm$ is simulated at an initial separation of $7.5\,\mu m$ from a GDL layer with the same area. In
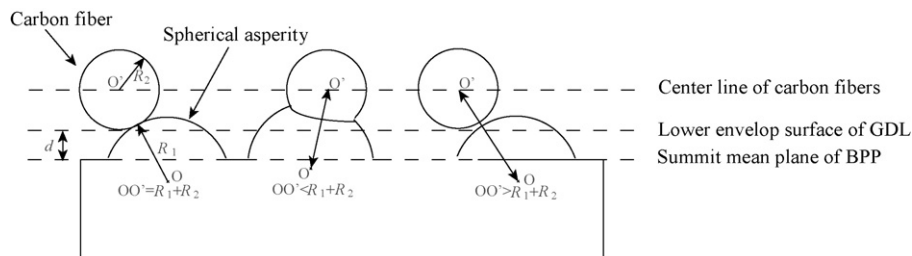


Fig. 5. Two-dimensional illustration of relative position between BPP asperities and carbon fibers.

Table 1
Material properties for the BPP and the GDL

| Properties | BPP | GDL |
|---|---|---|
| Thickness (mm) | 5 | 0.11 |
| Area (mm$^2$) | 101.6 × 101.6 | 100 × 100 |
| Porosity | | 80% |
| Young's modulus (GPa) | 10 | |
| Electrical resistivity-through plane ($\mu\Omega$ m) | 190 | 800 |

Table 2
Inputs parameters for the numerical contact model

| Parameters | Value |
|---|---|
| **BPP** | |
| Asperity peak density $D_{peak}$ (#mm$^{-1}$) | 98 |
| Summit radius $R$ ($\mu$m) | 3.67 |
| Summit standard deviation $\sigma_s$ ($\mu$m) | 3.55 |
| **GDL** | |
| Fiber diameter $d_{fiber}$ ($\mu$m) | 7 |
| Total fiber length $L_{fiber}^{tot}$ (mm mm$^{-2}$) | 572 |
| Fiber length in one layer $l_{fiber}$ (mm mm$^{-2}$) | 57 |

this study, the BPP is a grade FU 4369 graphite plate from PEM Technology Inc and the GDL is Toray TGP-H-030 from Toray Industries, Inc. All of the relevant material properties are listed in Table 1. Table 2 lists the inputs parameters for the numerical models. Parameters for BPP are obtained based on the profilometerical scans. Parameters for GDL are estimated from the GDL porosity and SEM micrographs. Other inputs to

the numerical model include carbon fiber material properties. The carbon fiber has more favorable mechanical and electrical properties in the longitudinal direction than in the transverse direction [4]. However, the transverse material properties have a more significant influence on the contact resistance in PEM fuel cells. Hence, such material properties are used in the numerical model. The transverse compressive modulus of Toray carbon fiber is 3.2 GPa [15]. The transverse electrical resistivity is 70 $\mu\Omega$ m, which is estimated using the Bruggman correlation [16],

$$\rho_1 = \rho_{GDL}(1 - \varepsilon)^{1.5} \qquad (12)$$

where $\rho_{GDL}$ is the through plane resistivity of the GDL.

Based on the simulated BPP surface and GDL structure, the relation between clamping pressure and contact resistances can be obtained by changing the separation.

### 3.2. Experimental validation

Experimental investigations were conducted to validate the numerical model results. Two experimental setups were built to measure the contact resistance [4,7,8]. Setup 1 as shown in Fig. 6(a) was built using a stack of a GDL and two graphite BPPs. This stack was inserted between two copper plate current collectors. Plexiglas plates were used for insulation. The measured resistance from Setup 1 includes the bulk resistances of two BPPs, the bulk resistance of GDL, contact resistances between cooper plates and BPPs, BPPs and GDL. Setup 2 uses a similar stack but with only one BPP between two copper plates in order to extract the contact resistance between BPP and GDL.
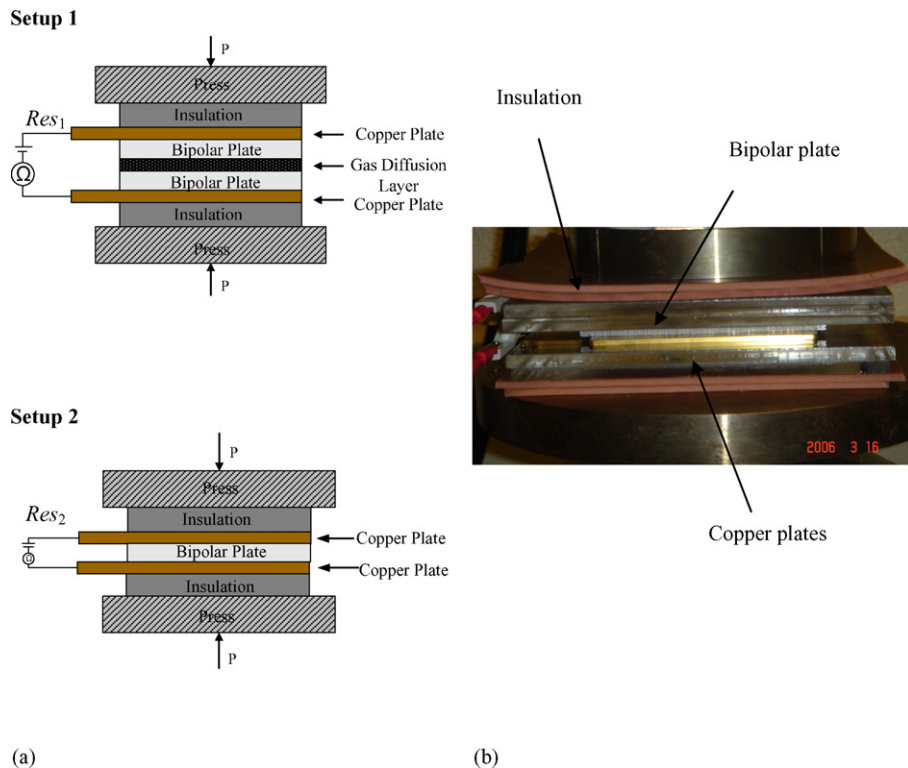


Fig. 6. (a) Schematic of two experimental setups and (b) picture of Setup 2.

An MTS machine was used to provide the clamping load and a DC milli-ohmmeter (GW-Instek GOM-802) was used to measure the resistance with a resolution of 0.1 μΩ.

The contact resistance between BPP and GDL can be deduced as [7]

$$R_{contact} = \frac{Res_1 - Res_2 - R_{BPP} - R_{GDL}}{2} \tag{14}$$

where $Res_1$ and $Res_2$ are measured resistances from Setups 1 and 2, respectively. $R_{BPP}$ is the bulk resistance of graphite BPP and $R_{GDL}$ is the bulk resistance of GDL. $R_{BPP}$ and $R_{GDL}$ are calculated according to their bulk resistivities. The change of the bulk resistance of BPP and GDL during compression is neglected. A series of compression pressures from 0.5 to 3 MPa were applied and the corresponding contact resistances were measured. Under each clamping pressure, the contact resistance measurements were repeated four times to obtain the average values. Two GDL samples are used and results are identified as Experiments 1 and 2.

## 4. Results and discussions

Results from the numerical model and experiments are presented in Fig. 7. Results from Experiments 1 and 2 are very comparable. The discrepancy between two experiments is less than 5%, which illustrates that the contact resistance measurement is repeatable. For every clamping pressure, the simulation was repeated five times. Results from repeated simulations show a small range of variability, in particular, when the clamping pressure becomes large. This is because, at high clamping pressure, the number of contact spots increases and the calculation is more accurate. The maximum relative error among different simulation runs is less than 3.5%. Furthermore, the numerical prediction shows the same trend as the experimental results and the difference is less than 20%. This consistency indicates that the numerical model captures reasonably well the contact phenomena between BPP and GDL in PEM fuel cells.

The number of contact spots increases rapidly when two contacting parts start to come into contact. The real contact area increases fast at this early stage because many asperities are coming into contact with the fibers. Thus, the contact resistance changes greatly during the initial clamping pressure increase as shown in Fig. 7. As the distance between two surfaces decreases further, only a few new asperities are becoming involved in the contact. Contact resistance decreases mainly due to the area increase of the existing contact spots. This slight increase of the contact area results in only small changes in the contact resistance. Although greater clamping pressure can reduce the contact resistance, high pressure may damage BPP, GDL and obstruct gas flow. From fuel cell performance prospective, electrical resistance and flow resistance need to be optimized simultaneously to obtain a proper clamping pressure.

In the numerical model, several assumptions were made to model BPP surface and GDL structure. In modeling the BPP surface roughness, the assumption of spherical asperities with identical radius is consistent with the G&W model. Some researchers have developed contact models with different asperity shapes and radii, but only shown that the G&W model is nevertheless quite accurate [10–12,17].

Although the length of each fiber is initially assumed to follow a uniform distribution, the final distribution will change after cutting. However, the different fiber length distributions after cutting will not change the total contact resistance. This is because BPP surface is a random surface, and every location of the GDL surface is statistically equivalent. To verify this numerically, a simplified GDL structure with the same total fiber length is modeled, in which all the fibers are in the horizontal direction. The difference between these two results is within 3%, therefore this assumption is reasonable.

The influences of BPP surface roughness parameters are also investigated. As shown in Fig. 8, when the peak density increases from 50 to 150 mm$^{-1}$, contact resistance decreases because more asperities are in contact. However, the contact resistance decreases about 14%, not as much as the change of peak density. For a given distance between two contacting surfaces, the larger summit density will result in an increased contact area and a smaller contact resistance, but larger clamping pressure is needed accordingly. In order to compare the resistances at dif-
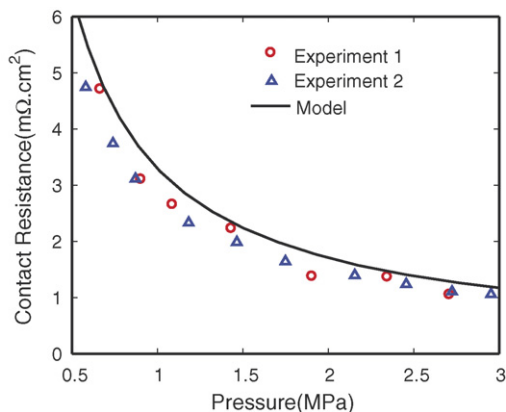


Fig. 7. Comparison of experimental data with numerical prediction.
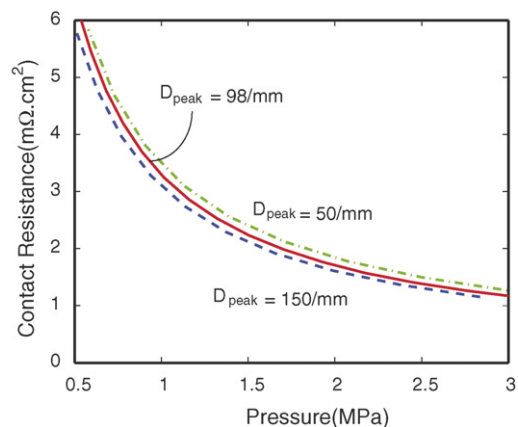


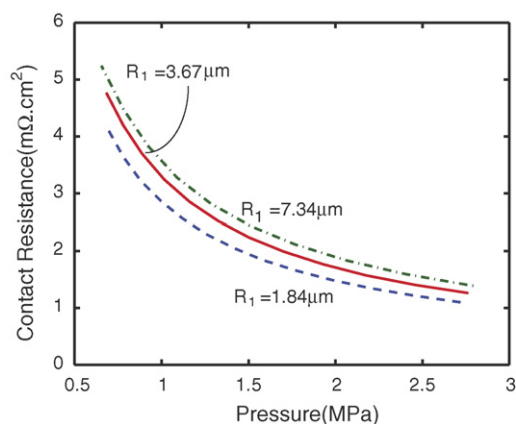Fig. 8. Influence of BPP summit density.
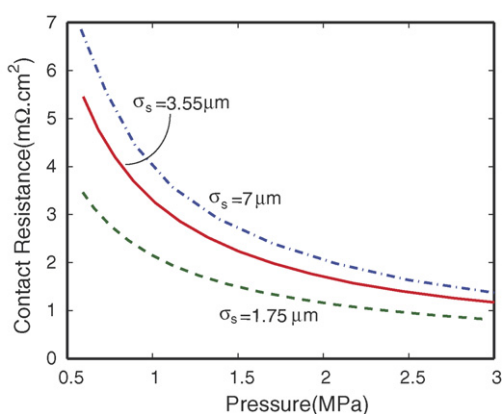
Fig. 9. Influence of BPP summit radius.



Fig. 10. Influence of BPP summit standard deviation.

ferent peak densities with a given pressure, the distance between the contact surfaces will be different. That is, smaller distance for low density and bigger distance for high density are required, respectively. The combined effect of the distance and the peak density makes the contact resistance not sensitive to the summit density changes. The contact resistance is also insensitive to summit radius change, as illustrated in Fig. 9.

The summit standard deviation of a BPP surface is another important surface roughness parameter. As shown in Fig. 10, when $\sigma_s$ changes from 3.55 to 7 µm, the contact resistance increases by about 20%. For the surface with $\sigma_s = 7$ µm, the likelihood to have high asperities is higher than that of smaller standard deviation. This results in the fact that the contact spot concentrates in a few asperities at the same clamping pressure. Thus, the contact area is smaller and the contact resistance turns out to be larger.

The contact resistance is more sensitive to summit standard deviation than summit density and summit radius. Hence, BPP surface should be fabricated with small standard deviation to ensure the consistency of contact resistance and the performance of PEM fuel cells.

## 5. Conclusions

A micro-scale contact model was developed to predict the contact resistance between BPP and GDL in PEM fuel cells. BPP surface roughness was simulated by adopting the classical statistical contact model and the GDL was modeled as randomly distributed fibers with estimated total fiber length. According to these two simulated contacting surfaces, contact spots between BPP and GDL can be determined numerically given a separation of these two surfaces. The contact status for every single contact spot was calculated using the Hertz theory. The total resistance and pressure were obtained by summarizing the results from each contact spot. Compared with experimental results, the modeling results showed good agreements with less than 20% discrepancy. Influences of BPP surface roughness parameters on contact resistance were also studied. It was found that the summit standard deviation has greater impact than other surface roughness parameters. The model developed in this study may be applied to predict the contact resistance of GDL in contact with other BPP materials, only if the GDL characteristics and BPP surface topology are determined. This micro-scale contact model is beneficial to understand the basic mechanisms of contact behavior between the rough surface and a fibrous medium and can be integrated with other fuel cell simulations to predict the overall fuel cell performance.

## References

[1] R.C. Makkus, A.H.H. Janssen, F.A. Bruijn, R. Mallant, J. Power Sources 86 (2000) 274–282.
[2] D.P. Davies, P.L. Adcock, M. Turpin, S.J. Rowen, J. Appl. Electrochem. 30 (2000) 101–105.
[3] S.J. Lee, C.D. Hsu, C.H. Huang, J. Power Sources 145 (2005) 53–361.
[4] M. Mathias, J. Roth, J. Fleming, W. Lehnert, in: W. Vielstich, A. Lamm, H.A. Gasteiger (Eds.), Handbook of Fuel Cells—Fundamentals, Technology and Applications, V3: Fuel Cell Technology and Application, Wiley, 2003, pp. 517–538.
[5] J. Ihonen, G. Lindbergh, G. Sundholm, Electrochim. Acta 46 (2001) 2899–2911.
[6] W. Lee, C. Ho, J. Zee, M. Murthy, J. Power Sources 84 (1999) 45–51.
[7] V. Mishra, F. Yang, R. Pitchumani, J. Fuel Cell Sci. Technol. 1 (2004) 2–9.
[8] L. Zhang, Y. Liu, H. Song, S. Wang, Y.Y. Zhou, S.J. Hu, Estimation of contact resistance in proton exchange membrane fuel cells based on experimental constitutive relation, J. Power Sources 162 (2006) 1165–1171.
[9] J.A. Greenwood, J.B.P. Williamson, Proc. R. Soc. Lond. A295 (1966) 300–319.
[10] P.R. Nayak, J. Lubr. Technol. 93 (1971) 398–407.
[11] A.W. Bush, R.D. Gibson, T.R. Thomas, Wear 35 (1975) 87–111.
[12] J.I. McCool, Wear 107 (1986) 37–60.
[13] K.L. Johnson, Contact Mechanics, Cambridge University Press, 1985, pp. 84–106.
[14] R. Holm, Electric Contacts Theory and Application, Springer-Verlag, New York, 1967, pp. 9–16.
[15] J.B. Donnet, T.K. Wang, S. Rebouillat, J. Peng, Carbon Fibers, Marcel Dekker, New York, 1998, p. 319.
[16] J. Bear, J.M. Buchlin, Modeling and Application of Transport Phenomena in Porous Media, Kluwer Academic Publishers, Boston, MA, 1991.
[17] J.I. McCool, J. Tribology 122 (2000) 96–502.